

Coherence time extension in $\text{Pr}^{3+}:\text{Y}_2\text{SiO}_5$ by self-optimized magnetic fields and dynamical decoupling

G. Heinze,^{*} C. Hubrich, and T. Halfmann[†]*Institut für Angewandte Physik, Technische Universität Darmstadt, Hochschulstraße 6, 64289 Darmstadt, Germany*

(Received 11 November 2013; published 15 May 2014)

Long coherence times are an essential prerequisite for implementations of quantum information technology. This requires techniques to control perturbing processes and hence prolong coherence times in quantum systems. In our work, we present systematic experimental investigations on prolongation of spin coherence times in a rare-earth ion-doped crystal. The approach is based on a combination of established coherence control techniques (i.e., zero first-order Zeeman shifts and simple dynamical decoupling), supported by automatic optimization of experimental control parameters, as well as precise characterization of the optimization loop and the strongly modified complex level structure by spin echoes and high-resolution Raman heterodyne spectroscopy. The spin-echo and Raman heterodyne data clearly prove successful optimization towards proper conditions of zero first-order Zeeman shifts, finally yielding a coherence time of 1 min, i.e., close to the theoretical limit set by the population lifetime in $\text{Pr}^{3+}:\text{Y}_2\text{SiO}_5$.

DOI: [10.1103/PhysRevA.89.053825](https://doi.org/10.1103/PhysRevA.89.053825)

PACS number(s): 42.50.Gy, 03.67.Pp, 76.30.Kg, 76.60.Lz

I. INTRODUCTION

Decoherence plays a crucial role in applications of quantum optics, as it typically destroys phase information (e.g., encoded in superpositions of quantum states). Thus, many recent efforts in the field have dealt with control mechanisms to cope with perturbing decoherence processes. Some prominent examples are, e.g., decoherence-free subspaces [1–3], quantum error correction codes [4,5], or dynamical decoupling [6–10]. Moreover, it was shown, that smart control of external magnetic fields can help reduce fluctuations [11] and, finally, prolong coherence times in different types of quantum systems [12–16].

In our work, we deal with investigations and implementations of decoherence control in $\text{Pr}^{3+}:\text{Y}_2\text{SiO}_5$. The latter and similar rare-earth-ion-doped crystals combine naturally long coherence times (which typically are reserved for atomic gases) with the large density of solids. This makes such doped solids very promising candidates for realistic implementations of quantum information technology [17]. Recently, we applied $\text{Pr}^{3+}:\text{Y}_2\text{SiO}_5$ for light and image storage by electromagnetically induced transparency (EIT). Decoherence control enabled us to obtain very long optical storage times of 42 s (defined by the $1/e$ decay of the stored signal) [18]. In particular we applied “zero first-order Zeeman shifts” (ZEFOZ) and dynamical decoupling to prolong the coherence time in the solid medium. ZEFOZ in the doped solid relies on preparation of appropriate level splittings, such that the new levels are less sensitive to decoherence processes induced by magnetic interactions with the host lattice [15,19]. Dynamical decoupling is based on fast rephasing of spin coherences (which, e.g., serve to store information) by sequences of radio-frequency (rf) pulses. In a simplified explanation, the pulses rephase an inhomogeneously broadened ensemble faster than perturbing decoherence processes occur. Thereby, the perturbations are effectively averaged out, and the coherence

time increases [7,9]. However, the control techniques depend critically upon the exact choice of the experimental parameters. As examples, coherence control by ZEFOZ requires precise control of the field strength and orientation, and dynamical decoupling suffers from fluctuations of the pulse area. To cope with such imperfections of experimental coherence control, we developed and applied an automatic procedure to determine optimized conditions for ZEFOZ in $\text{Pr}^{3+}:\text{Y}_2\text{SiO}_5$. The algorithm uses spin-echo experiments with optical readout to evaluate progress in the optimization. We note that we already used this approach for our EIT light-storage experiments but gave no details in the corresponding publication [18]. In our present work we provide now a detailed description of the automatic optimization loop and characterize its progress as well as the final result by spin echoes and spectroscopy. Hence, after determination of the optimized magnetic field, we use Raman heterodyne spectroscopy to monitor the modified, very complex hyperfine level structure in $\text{Pr}^{3+}:\text{Y}_2\text{SiO}_5$ and verify optimization towards proper conditions for ZEFOZ. The combination of optimized ZEFOZ and dynamical decoupling finally permits a prolongation of the coherence time in $\text{Pr}^{3+}:\text{Y}_2\text{SiO}_5$ from the initial value of 500 μs to 1 min. This is already quite close to the population lifetime of $T_1 \sim 100$ s in $\text{Pr}^{3+}:\text{Y}_2\text{SiO}_5$, which sets the ultimate limit.

II. EXPERIMENTAL SETUP AND DETECTION METHODS

The experiments are performed in a $\text{Pr}^{3+}:\text{Y}_2\text{SiO}_5$ crystal with a length of 3 mm and a dopant concentration of 0.05% praseodymium. The crystal is mounted in a liquid-helium cryostat and held at temperatures of about 4 K to reduce phononic excitations. Figure 1(a) shows the relevant part of the level scheme of a single Pr^{3+} ion. The optical transition between the electronic ground state $^3\text{H}_4$ and the excited state $^1\text{D}_2$ is at a wavelength of 605.98 nm. Without external magnetic field ($B = 0$), each electronic state consists of three doubly degenerate hyperfine states, which are labeled according to their magnetic quantum number ($m_I = \pm\frac{1}{2}, \pm\frac{3}{2}, \pm\frac{5}{2}$). The level spacing of the hyperfine states within an electronic state is in the range of 10 MHz. The population lifetime of the

^{*}Present address: ICFO — The Institute of Photonic Sciences, Barcelona, Spain; georg.heinze@physik.tu-darmstadt.de

[†]<http://www.iap.tu-darmstadt.de/nlq>

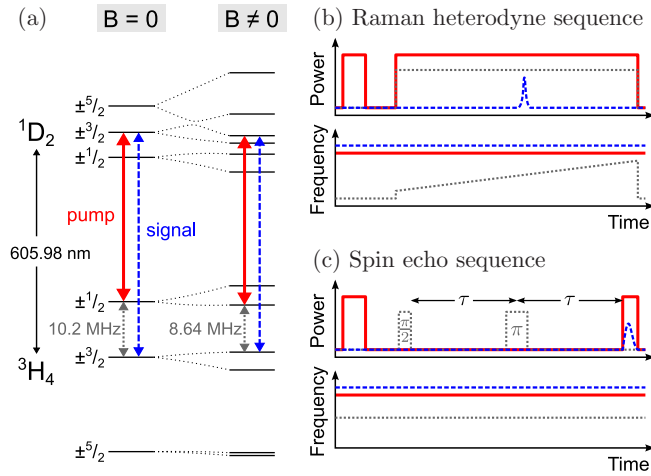


FIG. 1. (Color online) (a) Level scheme of a Pr^{3+} ion without external magnetic field ($B = 0$) and at \vec{B}_{ZEFOZ} ($B \neq 0$). (b) Schematic pulse sequence for Raman heterodyne spectroscopy. (c) Schematic pulse sequence for spin-echo experiments.

hyperfine states of the ground state $^3\text{H}_4$ is $T_1 \sim 100$ s [20]. The natural coherence time of these states is $T_2 \approx 500 \mu\text{s}$ [21,22].

If an external magnetic field is applied ($B \neq 0$), the hyperfine states split due to the Zeeman effect, depending upon the direction and strength of the external field \vec{B} . Following the notation introduced in Ref. [23], we orient the coordinate system with regard to the crystal axes $D1$, $D2$, and b such that $x \parallel D2$, $y \parallel D1$, and $z \parallel b$. The Zeeman level structure in $\text{Pr}^{3+}:\text{Y}_2\text{SiO}_5$ can be calculated from the effective quadrupole and Zeeman tensors [23,24]. As an example, Fig. 1(a) also shows the splitting in a specific magnetic field \vec{B}_{ZEFOZ} ($B \neq 0$), which we will discuss in more detail in Sec. III.

To characterize the Zeeman-shifted hyperfine structure of the Pr^{3+} ions, we apply Raman heterodyne spectroscopy [25,26] [see Fig. 1(b)]. First, an intense laser pulse (red solid line) optically pumps the populations in the $^3\text{H}_4$ hyperfine states. Second, we apply a long optical pump pulse and a coincident rf pulse with chirped frequency (gray dotted line). When the rf matches the frequency of a hyperfine transition in the $^3\text{H}_4$ manifold, it drives a spin coherence between the hyperfine states. The optical pump pulse scatters from the induced spin coherence and generates an optical Raman signal pulse (blue dashed line) at frequency $\omega_{\text{Sig}} = \omega_{\text{Pump}} \pm \omega_{\text{rf}}$. Due to the large inhomogeneous broadening of the optical transition in the gigahertz range, the pumping and Raman scattering processes take place in up to nine frequency ensembles of Pr^{3+} ions. Figure 1(a) shows an example of the coupling scheme in one specific ensemble. All ensembles contribute to a coherent signal pulse, which leaves the crystal in the same direction as the initial pump pulse. The beat note between the pump and the signal pulse reveals information about the spectral structure of the Pr^{3+} hyperfine states.

To measure the hyperfine coherence lifetime we apply a conventional spin-echo sequence, extended by optical preparation and detection [27,28] [see Fig. 1(c)]. First, a laser pulse optically pumps the hyperfine states of the Pr^{3+} ions. Afterwards, a rf pulse with a pulse area of $\pi/2$ drives a maximal coherence between two hyperfine states. After a time τ a rf

pulse with pulse area of π rephases the coherences in the inhomogeneously broadened ensembles. Hence, after the echo delay 2τ all spin coherences are in phase again to generate a large net coherence. An optical pump pulse scatters from the spin coherence and generates an optical signal pulse. The total energy of the signal pulse serves as a measure for the amplitude of the coherence in the medium at time 2τ . Decoherence processes reduce the amplitude of the spin coherence. Thus, observation of the signal pulse energy vs variation of the echo delay 2τ permits determination of the hyperfine coherence time. As in the case of the Raman heterodyne sequence, the signal pulse is detected as a beat note with the final pump pulse.

The experimental setup is as follows: A continuous-wave single-longitudinal-mode dye laser (Sirah Matisse DX) provides optical radiation at $\lambda = 605.98$ nm with a residual frequency jitter of about 100 kHz on a time scale of 100 ms. The laser radiation passes an acousto-optic modulator (AOM) which enables full control of temporal intensity and frequency profiles. Typical pump-laser powers behind the AOM are in the range of 10 to 100 mW. The beam diameter in the crystal is $\varnothing \approx 300 \mu\text{m}$. Two coils (diameter of 5 mm, five windings each), placed inside the cryostat around the crystal, are driven by amplified signals from an arbitrary waveform generator (AWG) to generate the required rf pulses. The maximum rf power is $P_{\text{rf}} = 10$ W. Three pairs of superconducting coils in orthogonal Helmholtz configuration, with diameters of a few centimeters, also placed in the cryostat around the crystal, serve to provide static magnetic fields of variable strength and direction in the crystal. With 200–400 windings on each coil and at a current of 10 A, we reach maximal magnetic fields of about 2000 G in each spatial direction. The coils are driven by high-power operational amplifiers (Servovatt DCP 390/20) which act as four-quadrant power supplies. On time scales of 100 ms we measured a relative fluctuation of the static magnetic-field strength of well below 10^{-4} . The long-term drift of the magnetic field over several hours was below 1 G. To detect the beat note between the pump and signal pulse (e.g., in the Raman heterodyne detection or the spin-echo experiments), we use a photodiode (Thorlabs PDA155-EC) and a lock-in amplifier (Zurich Instruments ZI HF2LI), with a locking reference from the AWG.

III. OPTIMIZING AND MONITORING CONDITIONS FOR ZEFOZ

The dominant source of decoherence of the Pr^{3+} hyperfine states is interactions with magnetic fields generated by the fluctuating spins of the Y ions in the crystal environment [29]. The changing magnetic fields lead to stochastic Zeeman shifts of the Pr^{3+} levels. As the phase of the coherence between two quantum states depends upon the level spacing, stochastic Zeeman shifts lead to decoherence.

We consider now application of a strong external magnetic field. If the field strength exceeds the Pr-Y magnetic dipole interaction strength, it defines a local quantization axis for the Y ions. This leads to reduced fluctuations of the Y spins and a lower interaction probability between the Pr and Y ions. It has been shown that already weak magnetic fields of some 10 G prolong coherence times from the initial value of $T_2 \approx 500 \mu\text{s}$ to the range of 10 ms [15,29]. A further reduction

of decoherence becomes possible if we use the strength and direction of stronger fields as control parameters. For stronger fields ($|\vec{B}| \gtrsim 100$ G) the Zeeman shift of the hyperfine states does not grow linearly with the magnetic-field strength any longer [see also Fig. 1(a)]. In this case, the Zeeman-shifted hyperfine levels show avoided crossings [15,23,24]. Thus, the dependence of the level energy vs the magnetic-field strength exhibits local maxima (or minima) for specific values of the magnetic field. This defines a ZEFOZ point, i.e., a specific choice \vec{B}_{ZEFOZ} of the magnetic field such that the frequency of a hyperfine transition is (to first order) independent of an external magnetic field $\Delta\vec{B}$. Hence, residual magnetic fluctuations (also inside the crystal) will not affect hyperfine spin coherences prepared under conditions of ZEFOZ, i.e., at \vec{B}_{ZEFOZ} . This permits a reduction of the perturbing Pr-Y magnetic dipole interactions and prolongation of the coherence time. The technique was first applied to Pr³⁺:Y₂SiO₅ in Refs. [15,30,31] to demonstrate a prolongation of the coherence time up to several hundred milliseconds.

However, a faithful reproduction of this result is not that simple as the ZEFOZ effect is extremely sensitive to an accurate tuning of the magnetic field. We adapted the values for the ZEFOZ point at $\vec{B}_{\text{ZEFOZ}} = (732, 173, 219)$ G, determined by Fraval *et al.* [15], and performed a spin-echo measurement on the corresponding hyperfine transition at 8.64 MHz in the electronic ground state ³H₄ [see Fig. 1(a) ($B \neq 0$)]. The temporal decay of the signal pulse energy E versus the echo delay 2τ at this initial choice \vec{B}_{start} for the ZEFOZ point is depicted in Fig. 3 as blue circles. The data are fitted with a nonexponential decay curve based on a phase-memory model [32]:

$$E(2\tau) = E_0 \exp \left[- \left(\frac{2\tau}{T_M} \right)^2 \right]. \quad (1)$$

For the sake of simplicity, in the following we will not refer to the phase-memory time T_M but will use the coherence time T_2 instead, i.e., the time after which the initial signal E_0 has dropped to $1/e$. The fit gives a coherence time of $T_2^{\text{start}} = 55$ ms, which is much shorter than the expected several hundred milliseconds at a perfect ZEFOZ point. This is due to slight misalignments of the crystal axes relative to the magnetic field, background fields, calibration errors, or other imperfections of the experimental setup. To determine the field for ZEFOZ under conditions of arbitrary variations in these or other experimental parameters, we implemented an automatic search algorithm and optimization loop.

The loop is based on a gradient search and works as follows: In step (a) we initialize the algorithm with a starting magnetic field \vec{B} and an expected hyperfine transition frequency ν_{rf} . As starting parameters we typically choose theoretically predicted magnetic fields for ZEFOZ points or results of previous experiments in other setups. In principle, it is also possible to start with an arbitrary choice or rough guess. In step (b) the search loop changes the magnetic field \vec{B} along the three spatial directions \vec{e}_i ($i = x, y, z$) by a small amount $\pm\Delta B$. In step (c) the experimental algorithm performs a Raman heterodyne experiment to determine the Zeeman-shifted resonance frequency $\nu_{\text{rf}}(\vec{B} \pm \Delta B \vec{e}_i)$ of the relevant hyperfine transition. In step (d) the loop conducts a resonant

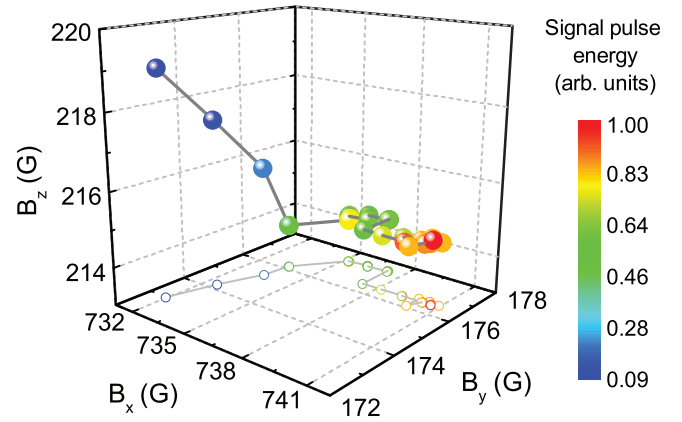


FIG. 2. (Color online) Evolution of the magnetic field during the automatic optimization loop to determine the optimal ZEFOZ point. The loop applies Raman heterodyne spectroscopy and spin echoes to evaluate progress towards longer coherence times. Each data point indicates the result of one iteration step in the algorithm. The algorithm runs through 33 iterations before it converges to the optimal magnetic field, indicated by the red dot.

spin-echo experiment at $\nu_{\text{rf}}(\vec{B} \pm \Delta B \vec{e}_i)$ to determine the effect of the new magnetic field upon the coherence time. To speed up the optimization process, the algorithm records the spin-echo signal at a single fixed echo delay, rather than varying the echo delay 2τ to measure the entire coherence decay. The results of steps (b)–(d) yield information about the gradient of the coherence time with regard to the magnetic-field vector. The loop calculates this gradient in step (e) and determines in which spatial direction we must change the magnetic field by a step $\pm\Delta B$ to obtain the steepest increase in coherence time. The new field is the start value for the next iteration of the optimization loop, starting again with step (a).

Figure 2 shows the progress of the optimization loop in a typical experiment. The algorithm started at a calculated magnetic field of $\vec{B}_{\text{start}} = (732, 173, 219)$ G (blue dot) and converged towards $\vec{B}_{\text{end}} = (741, 177, 215)$ G (red dot). The initial step size ΔB of the magnetic field was 2 G to enable quick optimization in the first iterations. During optimization the algorithm gradually reduced the grid size to $\Delta B = 0.2$ G for fine-tuning of the magnetic field in the last iterations. The loop required a runtime of 30 min only. The plot shows a systematic optimization path through the magnetic field parameter space towards best conditions for ZEFOZ in our setup. As expected the signal pulse energy (and hence the coherence time) steadily increases during optimization.

To determine the finally obtained coherence time, we recorded the variation of the spin-echo signal vs the echo delay time (see Fig. 3). The graph shows the decay of the signal pulse energy in the echo under conditions of the initial field $\vec{B}_{\text{start}} = (732, 173, 219)$ G (blue circles), as well as for the optimized field $\vec{B}_{\text{end}} = (741, 177, 215)$ G. In addition to the data points, we also plot decay functions according to Eq. (1). At the final ZEFOZ configuration \vec{B}_{end} we obtain a $1/e$ coherence time of $T_2^{\text{opt}} = 392 \pm 14$ ms. This is roughly a factor of 800 longer compared to the natural coherence time ($T_2 \approx 500 \mu\text{s}$) and a factor of 8 longer compared to the case of the theoretically calculated ZEFOZ point. Thus, although

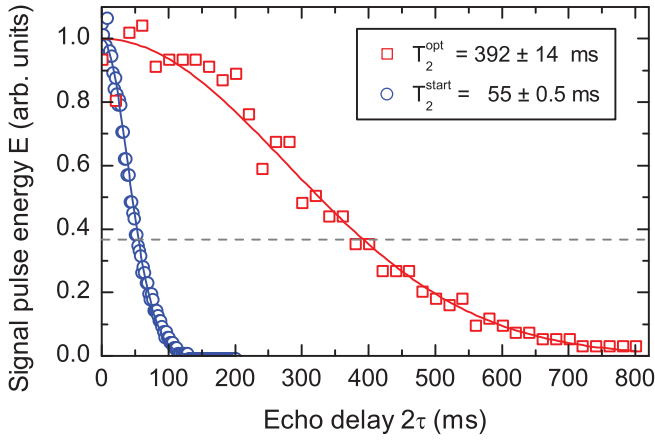


FIG. 3. (Color online) Variation of the signal pulse energy vs echo delay time for the case of the initial magnetic field $\vec{B}_{\text{start}} = (732, 173, 219)$ G (blue circles) and the optimized field $\vec{B}_{\text{end}} = (741, 177, 215)$ G (red squares). Solid lines represent fits based on Eq. (1), yielding $1/e$ coherence times of $T_2^{\text{start}} = 55$ ms and $T_2^{\text{opt}} = 392$ ms. The $1/e$ level is indicated in the graph by a gray dashed line.

the optimized magnetic field differs only by $\sim 1\%$ (depending on the field component) from the initially calculated value, the coherence time increases almost by an order of magnitude. This confirms that very precise determination of the ZEFOZ conditions is crucial to obtain long coherence times. This is important for any new experimental setup which aims at ZEFOZ, any change in such a setup, or even effects of daily fluctuations in the laboratory environment. Precise optimization of the ZEFOZ point (in our case with accuracies in the range of well below 1%) is required in all these cases. Finally, we must not fail to mention that in a similar ZEFOZ experiment in $\text{Pr}^{3+}:\text{Y}_2\text{SiO}_5$ coherence times up to ~ 900 ms have been reported [30,31]. This may be due to a stronger noise in our magnetic-field setup or a larger inhomogeneity of background fields in our setup, which we cannot compensate with the applied Helmholtz coils. Nevertheless, our optimization loop surely determines the best conditions for ZEFOZ which are possible in the setup.

To further verify the conditions for ZEFOZ at the optimized magnetic field, we applied Raman heterodyne spectroscopy to record Zeeman spectra of the complicated, modified hyperfine structure in the electronic ground state $^3\text{H}_4$ vs the magnetic-field strength (see Fig. 4). We change the magnetic field by steps of 5 G in the range of ± 250 G around the optimized ZEFOZ point at $\vec{B}_{\text{end}} = (741, 177, 215)$ G. For each of the three graphs in Fig. 4 we keep two spatial field components fixed at their optimized values while we vary the other field component. The rf was continuously swept from $\nu_{\text{rf}} = 1$ to 20 MHz during time intervals of 1 s. The contour plot of the experimental data clearly reveals the nonlinear dependence of the energy levels upon the magnetic-field strength. At the optimized configuration \vec{B}_{end} we observe the expected vanishing first-order derivative of the energy shift (marked by white crosses). The measured hyperfine transition frequency of $\nu_{\text{rf}} = 8.636$ MHz agrees very well with our simulations and previous experiments [15].

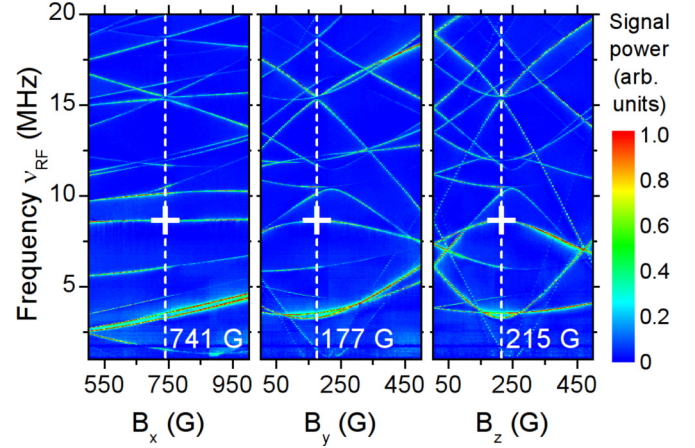


FIG. 4. (Color online) Zeeman spectra of the ground-state hyperfine structure around the optimized ZEFOZ point \vec{B}_{end} , measured by Raman heterodyne spectroscopy. Variation of the transition frequency vs magnetic-field strength in the x, y, z direction. Color coding in the contour plot indicates Raman signal powers. For each graph one component of the magnetic field was varied while the other two components were kept fixed. Thus, in the left graph the (y, z) field components were set to $B_y = 177$ G and $B_z = 215$ G while the component B_x was varied. In the middle graph, the (x, z) field components were set to $B_x = 741$ G and $B_z = 215$ G. In the right graph, the (x, y) field components were set to $B_x = 741$ G and $B_y = 177$ G. The white crosses indicate the ZEFOZ point.

IV. FURTHER EXTENSION OF COHERENCE TIMES BY DYNAMICAL DECOUPLING

To further extend the coherence time in $\text{Pr}^{3+}:\text{Y}_2\text{SiO}_5$, we combine the now optimized ZEFOZ with dynamical decoupling. The latter was initially developed in nuclear magnetic resonance [28,33,34], but in recent years it has also become popular in quantum information science [35–37]. In contrast to the more passive ZEFOZ approach, dynamical decoupling can be understood as an active protection of the quantum system. In dynamical decoupling the quantum system is driven by a large number of fast rephasing processes to suppress phase fluctuations of coherence due to stochastic interaction with the environment. The cycling time (i.e., the delay between two subsequent rephasing processes) must be short compared to the correlation time in the medium, i.e., the typical time scale of changes in the environment. In the simplest experimental case in $\text{Pr}^{3+}:\text{Y}_2\text{SiO}_5$, dynamical decoupling is essentially an extension of conventional rephasing by fast, repeated application of a multitude of identical π pulses. Thus, in our experiment we replaced the single rf π pulse of the Hahn spin-echo sequence [see Fig. 1(b)] by a large number N of such pulses, separated by the cycling time $T_C = 2\tau$. In this case, the total echo delay time is $N \times 2\tau$. If the cycling time is shorter than the reconfiguration of the surrounding Y^{3+} ions, it effectively decouples the Pr^{3+} ions from environmental noise.

Figure 5 shows the result of spin-echo experiments at the optimized ZEFOZ configuration $\vec{B}_{\text{end}} = (741, 177, 215)$ G combined with dynamical decoupling sequences of different cycling times $T_C = 100$ ms, 50 ms, 1 ms, and 100 μs . The large number of up to several thousand rephasing processes

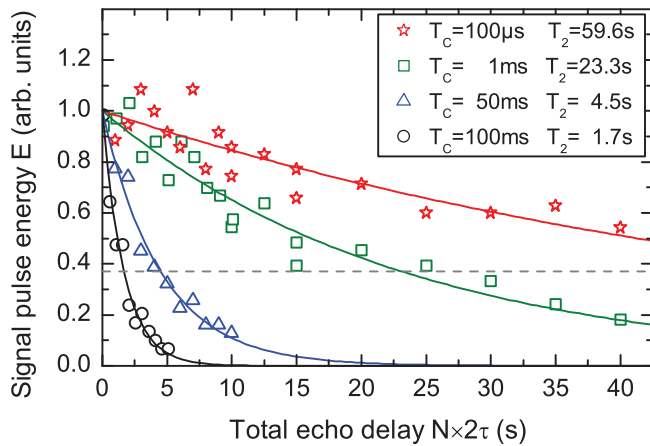


FIG. 5. (Color online) Variation of the signal pulse energy vs total echo delay time at the optimized ZEFOZ configuration B_{end} combined with dynamical decoupling for different cycling times. Solid lines represent fit functions according to a simple exponential decay.

during a single experiment modifies the temporal shape of the spin-echo decay. The effect of the successively applied π pulses adds up independently, such that the double-quadratic decay of the spin-echo signal according to the phase-memory model [see Eq. (1)] no longer holds. Instead, in the case of sufficiently short cycling times T_C , the temporal dependence reduces to a simple exponential decay curve [38] (as indicated by solid lines in Fig. 5). The combination of ZEFOZ and dynamical decoupling prolongs the coherence times towards the range of seconds. As expected, decoupling works better for shorter cycling times T_C , i.e., faster decoupling from the noisy environment. For the shortest cycling time $T_C = 100 \mu\text{s}$ we observe a $1/e$ coherence time of 1 min. This is the longest coherence time measured so far in Pr³⁺:Y₂SiO₅. It exceeds the best previous demonstration by a factor of 2 [30]. We note that in contrast to the previous work, our setup for dynamical decoupling does not seem to suffer much from error accumulations due to pulse area fluctuations in the π pulses. The latter limit the effect of dynamical decoupling, which can even lead to a decrease in the coherence time for faster decoupling (i.e., at shorter cycling times). In our experiment, this is not yet the case. This permitted us to further prolong the coherence times by reducing the cycling time to $T_C = 100 \mu\text{s}$.

V. CONCLUSION

We investigated optimized control of coherence processes between hyperfine spin states in a rare-earth-ion-doped solid by application of zero first-order Zeeman shifts and dynamical decoupling. The investigations are based on radio-frequency spin-echo experiments in Pr³⁺:Y₂SiO₅, involving optical readout and detection by Raman heterodyne spectroscopy. To optimize conditions for ZEFOZ, we applied an automatic optimization loop, involving an experimental gradient search algorithm. The loop serves to determine the optimal three-dimensional magnetic field for ZEFOZ. Spin-echo signals provide a measure to determine the progress of the optimization loop. We determined an optimal field of $\vec{B} = (741, 177, 215)$ G with a precision in the range of very well below 1%. From the spin-echo experiments we found this precision crucial to reach long coherence times. A deviation of the magnetic-field strength in the range of 1% does otherwise reduce the achieved coherence time by almost an order of magnitude. To confirm optimal preparation of ZEFOZ conditions, we applied Raman heterodyne spectroscopy to record the complicated, nonlinear multilevel Zeeman splittings around the ZEFOZ point with high precision. The spectra confirmed the expected first-order variation of the hyperfine transition frequency with the external magnetic field. Finally, we combined ZEFOZ with dynamical decoupling, driven by Carr-Purcell sequences of rephasing rf π pulses. When the time delay between the π pulses is sufficiently short, the rf rephasing pulses effectively decouple the quantum system from the environment. We obtained coherence times up to 1 min, i.e., the longest value measured so far in Pr³⁺:Y₂SiO₅. As rare-earth-ion-doped crystals are promising candidates for key components of quantum information technology, our findings on optimized ZEFOZ control of decoherence therein are of relevance to quantum storage protocols in such media.

ACKNOWLEDGMENTS

The authors thank D. Schraft and S. Mieth for experimental support and J.-L. Le Gouët for valuable discussions. The research leading to these results has received funding from the Deutsche Forschungsgemeinschaft and the People Programme (Marie Curie Actions) of the European Union's Seventh Framework Programme FP7/2007-2013/ under REA Grant Agreement No. 287252.

- [1] P. Zanardi and M. Rasetti, *Phys. Rev. Lett.* **79**, 3306 (1997).
- [2] D. A. Lidar, I. L. Chuang, and K. B. Whaley, *Phys. Rev. Lett.* **81**, 2594 (1998).
- [3] D. Lidar and K. Whaley, in *Irreversible Quantum Dynamics*, edited by F. Benatti and R. Floreanini (Springer, Berlin, 2003), pp. 83–120.
- [4] P. W. Shor, *Phys. Rev. A* **52**, R2493 (1995).
- [5] D. G. Cory, M. D. Price, W. Maas, E. Knill, R. Laflamme, W. H. Zurek, T. F. Havel, and S. S. Somaroo, *Phys. Rev. Lett.* **81**, 2152 (1998).
- [6] L. Viola and S. Lloyd, *Phys. Rev. A* **58**, 2733 (1998).
- [7] L. Viola, E. Knill, and S. Lloyd, *Phys. Rev. Lett.* **82**, 2417 (1999).
- [8] L. Viola, *J. Mod. Opt.* **51**, 2357 (2004).
- [9] W. Yang, Z.-Y. Wang, and R.-B. Liu, *Front. Phys.* **6**, 2 (2011).
- [10] A. M. Souza, G. A. Álvarez, and D. Suter, *Philos. Trans. R. Soc. A* **370**, 4748 (2012).
- [11] A. Smith, B. E. Anderson, S. Chaudhury, and P. S. Jessen, *J. Phys. B* **44**, 205002 (2011).
- [12] J. J. Bollinger, D. J. Heizen, W. M. Itano, S. L. Gilbert, and D. J. Wineland, *IEEE Trans. Instrum. Meas.* **40**, 126 (1991).
- [13] D. M. Harber, H. J. Lewandowski, J. M. McGuirk, and E. A. Cornell, *Phys. Rev. A* **66**, 053616 (2002).

- [14] C. Langer, R. Ozeri, J. D. Jost, J. Chiaverini, B. DeMarco, A. Ben-Kish, R. B. Blakestad, J. Britton, D. B. Hume, W. M. Itano, D. Leibfried, R. Reichle, T. Rosenband, T. Schaetz, P. O. Schmidt, and D. J. Wineland, *Phys. Rev. Lett.* **95**, 060502 (2005).
- [15] E. Fraval, M. J. Sellars, and J. J. Longdell, *Phys. Rev. Lett.* **92**, 077601 (2004).
- [16] S. Olmschenk, K. C. Younge, D. L. Moehring, D. N. Matsukevich, P. Maunz, and C. Monroe, *Phys. Rev. A* **76**, 052314 (2007).
- [17] C. Simon *et al.*, *Eur. Phys. J. D* **58**, 1 (2010),
- [18] G. Heinze, C. Hubrich, and T. Halfmann, *Phys. Rev. Lett.* **111**, 033601 (2013).
- [19] M. Lovrić, P. Glasenapp, D. Suter, B. Tumino, A. Ferrier, P. Goldner, M. Sabooni, L. Rippe, and S. Kröll, *Phys. Rev. B* **84**, 104417 (2011).
- [20] M. Nilsson, L. Rippe, S. Kröll, R. Klieber, and D. Suter, *Phys. Rev. B* **70**, 214116 (2004).
- [21] B. S. Ham, M. S. Shahriar, M. K. Kim, and P. R. Hemmer, *Opt. Lett.* **22**, 1849 (1997).
- [22] G. Heinze, S. Mieth, and T. Halfmann, *Phys. Rev. A* **84**, 013827 (2011).
- [23] M. Lovrić, P. Glasenapp, and D. Suter, *Phys. Rev. B* **85**, 014429 (2012).
- [24] J. J. Longdell, M. J. Sellars, and N. B. Manson, *Phys. Rev. B* **66**, 035101 (2002).
- [25] J. Mlynek, N. C. Wong, R. G. DeVoe, E. S. Kintzer, and R. G. Brewer, *Phys. Rev. Lett.* **50**, 993 (1983).
- [26] N. C. Wong, E. S. Kintzer, J. Mlynek, R. G. DeVoe, and R. G. Brewer, *Phys. Rev. B* **28**, 4993 (1983).
- [27] E. L. Hahn, *Phys. Rev.* **80**, 580 (1950).
- [28] H. Y. Carr and E. M. Purcell, *Phys. Rev.* **94**, 630 (1954).
- [29] E. Fraval, M. Sellars, A. Morrison, and A. Ferris, *J. Lumin.* **107**, 347 (2004).
- [30] E. Fraval, M. J. Sellars, and J. J. Longdell, *Phys. Rev. Lett.* **95**, 030506 (2005).
- [31] S. E. Beavan, E. Fraval, M. J. Sellars, and J. J. Longdell, *Phys. Rev. A* **80**, 032308 (2009).
- [32] W. B. Mims, *Phys. Rev.* **168**, 370 (1968).
- [33] S. Meiboom and D. Gill, *Rev. Sci. Instrum.* **29**, 688 (1958).
- [34] J. S. Waugh, *J. Magn. Reson.* (1969) **50**, 30 (1982).
- [35] M. J. Biercuk, H. Uys, A. P. VanDevender, N. Shiga, W. M. Itano, and J. J. Bollinger, *Nature (London)* **458**, 996 (2009).
- [36] A. M. Souza, G. A. Álvarez, and D. Suter, *Phys. Rev. Lett.* **106**, 240501 (2011).
- [37] T. van der Sar, Z. H. Wang, M. S. Blok, H. Bernien, T. H. Taminiau, D. M. Toyli, D. A. Lidar, D. D. Awschalom, R. Hanson, and V. V. Dobrovitski, *Nature (London)* **484**, 82 (2012).
- [38] M. F. Pascual-Winter, R.-C. Tongning, T. Chanelière, and J.-L. Le Gouët, *Phys. Rev. B* **86**, 184301 (2012).